TECHNICAL REPORT NO. 12

VOID VOLUMES IN SUBCOOLED BOILING SYSTEMS

PETER GRIFFITH
JOHN A. CLARK
WARREN M. ROHSENOW

THE OFFICE OF NAVAL RESEARCH
CONTRACT N5ori-07894
NONR-1848 (39)
D.S.R. PROJECT NUMBER 7-7673

MARCH 1, 1958

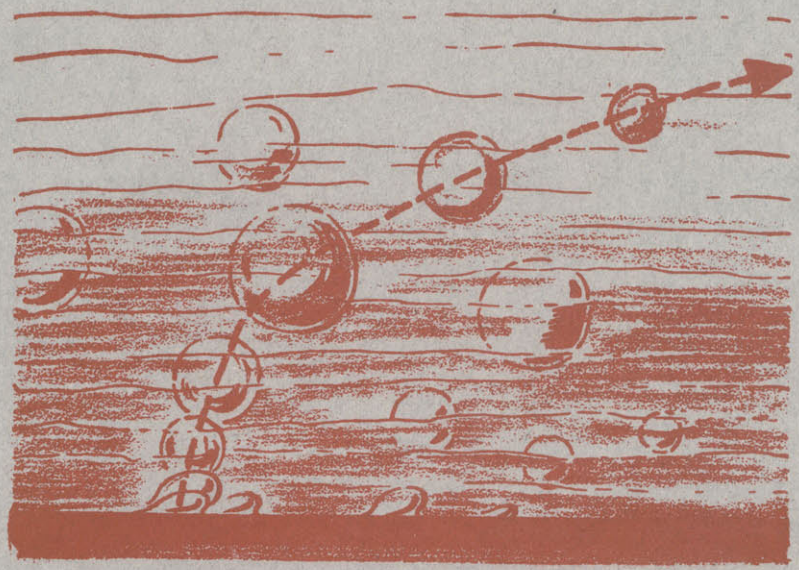

MASSACHUSETTS INSTITUTE OF TECHNOLOGY
DIVISION OF INDUSTRIAL COOPERATION
CAMBRIDGE 39, MASSACHUSETTS

VOID VOLUMES IN SUBCOOLED BOILING SYSTEM

Peter Griffith, John A. Clark, and
Warren M. Rohsenow

INTRODUCTION

Knowledge of the pressure drop in a channel and the resulting flow redistribution is essential in predicting the performance of a nuclear reactor. The pressure drop in a channel which is experiencing boiling is, in part, dependent on the void volumes present. In this report the results of an experimental investigation of the void volumes in systems at 500, 1000, and 1500 psia are presented. A method of predicting the void volumes is then presented. Finally, a comparison of measured and predicted void volumes is made with data collected at 2000 psia under completely different conditions. Agreement with the data is very good.

I THE EXPERIMENTAL PROGRAM

The objective of the experimental program was to determine the void volume in a subcooled boiling system. Basically the procedure used was to fix the heat flux, velocity and pressure on a surface in boiling and photograph it. The bubbles on the photograph were then measured, and counted and the void volume calculated.

A. Description of Test Apparatus

Figure 1 is a schematic diagram of the complete system for the visual boiling studies. As is shown in the above figure the visual system included the windowed stainless steel test section mounted on a vertical axis, a circulating pump, two system water preheaters, a calibrated orifice, a pressure vessel, and an ion exchanger. Power to the terminals of the heater strip which was installed in the visual test section was supplied by two 12 volt, 3000 ampere DC generators.

Thermocouples, as is shown in Figure 1, were installed in the visual system at the inlet and outlet of the test section, at the orifice location, and on either side of each preheater unit. The junctions of the above mentioned thermocouples were assembled from AWG #26 Chromel P and constantan calibrated wires. Copper wire leads from the ice junction were used to complete the electrical circuit to the switchbank outside the test cell. Additional thermocouples were installed on the resistance strips and between the coils of the two preheaters to permit a check on the high temperature surfaces of the units. The high temperature thermocouples were constructed from AWG #18 Chromel and Alumel calibrated wires with copper leads from the ice bath terminals to the switchbank.

System pressure was recorded on a Bourdon type Heise gage, 0-2000 psig, which connected into the system immediately upstream of the visual test section.

Flow measurements were recorded by means of a Barton Differential Pressure Gage, 0-100 inches of water, connected across the visual orifice plate.

Pressure vessel liquid level measurements were recorded on a Barton Differential Pressure Gage with a reversed reading scale, 50-0 inches of water. The gage taps connected to the bottom of the pressure vessel and to a reference water leg.

Voltage drop across the heater strip was determined by electrical metering instruments which connected to two AWG #10 Chromel wire leads from the test section. One lead was soldered to the high voltage side of the heater strip while the other was connected through the test section frame to the grounded side of the heater strip.

Heater strip current was metered by means of the voltage drop across a calibrated shunt resistance which was positioned in series with the test

section power circuit.

Photographic data were taken with a 4 x 5 inch Graphic View Still Camera with a Wollensak Rapter, 162 mm., f/4.5 lens - shutter attachment. The camera was mounted on a rigid steel frame which had been installed in the test cell. The light source used was a General Radio Microflash type 1530 - A with gas filled lamp tube. Kodak 4 x 5 inch Panatomic-X negative sheet film was used.

B. Operation of Test Apparatus

The system was degassed and the desired pressures and temperatures set. After the Microflash lighting unit and the Graphic View Still Camera had been set up for density or top view pictures, the heater strip power was turned on and increased to the point where the first trace of boiling for the particular combination of pressure, temperature, and test section water velocity conditions was observed on the frosted viewing plate of the camera. At this power setting or heat flux the appropriate lens aperture was selected after which ten consecutive pictures were taken by an operator in the test cell. Data representing two increased values of heat flux, usually taken at intervals of 50 amperes above the lowest power setting were obtained for the same combination of system conditions.

A 550°F temperature maximum was not exceeded since previous experience at conditions above this point resulted in repeated quartz window breakage and gasket failure presumably due to both the high temperature level and excessive gradients.

The negative film containing density data was developed in the darkroom in batches of 48 sheets. Chemical processing during the phase of development was controlled as closely as possible to insure uniformity between film batches. The photographic prints were processed with the idea in mind that the basic density data were contained on the negative film; hence,

enlarger settings, print exposure times, and the types of photographic paper used were selected on the basis of the best possible reproduction of the negative data rather than from uniformity considerations.

C. Test Section

The visual test section was machined from a solid piece of stainless steel stock and includes in addition to the compartment supporting the window sections a heavy length of inlet pipe the purpose of which is to stabalize the flow before entrance into the transparent portion of the test section. The flow channel is a square section 0.500 inches on a side extending throughout the entire length of test section. Close tolerances for the flow channel were made possible by machining a 0.500 inch slot in the test section parallel to the flow direction thus forming three of the four channel walls. The fourth wall was placed by welding a 0.500 inch plate in the above slot and machining the plate overlap flush with the external surface of the test section. The visual test section is secured in the system by means of two Van Stone flanges welded to the ends of the inlet and outlet pipes. Figure 2 shows the flanges, entrance pipe, and the window compartment of the visual test section. Immediately upstream of the transparent portion of the test section are positioned a chromel-constantan thermocouple hot junction and a static pressure tap. The pressure tap is connected to a bourdon type Heise pressure gage 0-2000 psi which records the gage pressure of the visual system. An additional chromel-constantan thermocouple is positioned immediately downstream of the window compartment.

Each of the three windows of the visual test section measure 3/4 x 3/4 x 4 inches with a 3/8 inch radius on each end. For the majority of the data taken, fused quartz windows were used, although for runs below 450°F pyrex units were installed to reduce quartz depreciation. The windows were

sealed from high pressures by means of a pair of buna-n rubber O-rings installed in such a manner as to position the seal on the continuous side surface of each window. The rubber packing was contained within the volume bounded by the test section frame, the side surface of the window, and a packing ring which surrounded the window. By means of adjustment screws the steel ring could be made to exert on the packing high compressive stresses which in turn forced the O-ring material against the side surface of the window with sufficient pressure to provide the necessary sealing surface. Figure 3 indicates in a cross-sectional view on a horizontal plane the relative positions of windows, packing, and stainless steel ring. Not shown in this figure is a copper wire ring which was installed around each of the windows in much the same manner as the O-rings. The copper ring was positioned in the corner formed by the test section frame and the window and was backed up by the window packing. In this manner the packing material could not extrude under pressure into the flow channel. The low pressure face of each window was supported by the ring of metal surrounding the oval-shaped eye piece of the test section frame. The supporting surface was machined to very close flatness tolerances and backed up by two heavy stainless steel plates in order to guard against stress concentrations in the window material due to irregularities of the supporting surface. The flatness tolerances for the finished windows were of the same order of magnitude as those for the supporting surface. Since only one light source was used, thus requiring the use of only two of the three windows in the test section, the window opposite the lighting window on the top view photographs was replaced with a stainless steel plug of the same dimensions as the windows. Grids were machined in the plug surface facing the light source and the surface electropolished to insure the reflection of incident light to the surface of the heater strip.

Figure 4 is a photograph of the window supporting frame assembly showing the frame, packing adjustment ring, quartz window, and the copper wire ring. Figure 5 is a photograph of the window frame as viewed from outside the test section. Figure 6 is a photograph of the stainless steel reflector plug showing the gridded and polished reflector surface.

In the window compartment of the visual test section three of the flow channel walls are formed by the surfaces of the two transparent windows and the stainless steel reflector plug. The surface of the heater strip forms the fourth wall of the flow channel. The heater strip itself is supported by a heavy stainless frame around which is employed a seal identical with that of the windows. The back plate or heater strip supporting frame aligns the heater surface in a vertical plane parallel to the direction of water flow. Across the length of heater strip is imposed a DC voltage introduced through an electrically insulated terminal which extends from the positive side of the heater strip through the back plate to the exterior of the visual test section. The ground side of the strip contacts the frame which is connected to a ground lead returning to the low voltage side of the power source. The electrically positive side of the heater strip is insulated from the grounded frame by thin sheets of mica. Insulated from and along each side of the heater strip are fastened two side strips which act as supports for the thinned length of the heater strip. Figure 7 is a side view of the heater strip showing its geometry and dimensions. It will be noted that the two terminals of the strip itself are of such geometry that they contribute little to the overall resistance of the strip. By virtue of the electrical work the heating power of the strip is concentrated over the thinned portion. Figure 8 shows the relative positions of heater strip, side strips, and mica insulation in addition to the direction of system water flow, lighting

axis for density or top view pictures, and the position of the index notches which are filed in the side strips for print orientation. Figure 9 is a photograph of the back plate assembly showing the heater strip, index notches, supporting frame for the heater strip, and the short rod which serves as the positive terminal of the test section heating unit. Also shown in the photograph is a potential tap lead extending from the longer tube. The wire leading out of the tube is soldered to the high voltage side of the heated length of the heater strip while a second wire is grounded to the frame. The wires are connected to a resistive circuit by means of which their electrical potential difference may be measured. At the end of the long tube a water jacket provides cooling for the pressure seal located at that position in the tube. Figure 2 shows the window frames secured in place on the body of the visual test section. The backplate assembly which is bolted to the back side of the test section is obscured from view.

D. The Analysis of the Data

At each setting of velocity, subcooling, pressure and heat flux, ten pictures were taken. The film was developed and printed and the four most representative pictures for that particular set of conditions were selected for counting and measuring. The procedure was as follows. For analysis a small portion of the heater strip was chosen near its upstream end. (See Figures 7 and 8.) The size of this portion, "the area of interest," was 1/2 inch long by 1/2 inch wide. Of the 1/2 inch width 3/8 inch was heater surface and 1/8 inch was electrical insulation on either side. First the magnification was found for that particular picture by measuring the distance between known marks on the surface. The area of interest was then broken down into smaller areas to facilitate the analysis. The vapor bubbles were first counted and tabulated regardless of size. Then each

vapor bubble 0.01 inch in diameter and greater on the print was measured to the nearest 0.01 inch and the number of bubbles at each diameter tabulated. All the remaining bubbles were grouped as having a 0.005 inch diameter. In all cases the contribution of these very small bubbles to the total vapor volume was negligible. Summation of the cubed diameters times the number of bubbles at each diameter times an appropriate conversion factor provided the vapor volume generated at a given condition.

For given values of pressure, velocity and heat flux there is a certain value of the bulk temperature at which boiling will just begin. This value depends on the film coefficient at the surface. In order to determine what value this was, the film coefficient for the heater surface was calculated using the equation presented below. This equation was found to give values of incipient boiling heat flux which were closest to those actually observed (4, 5).

$$N_{Nux} = 0.036(N_{Rex})^{0.8}(N_{Pr})^{1/3} \qquad (1)$$

It appears that the appropriate length to use in the Reynolds and Nussalt numbers is the length from entrance to the area in question as the area of interest is so close to the entrance. The values of the film coefficient calculated with this equation and the temperatures for incipient boiling calculated are also presented in Table II at the end of this section.

E. Presentation of the Data

The experimentally determined void volumes are presented in Table I along with all the conditions under which they were obtained. Each point is the average of the four points analyzed. They are compared with values calculated using a procedure explained later in the report. Figures 10 through 13 are four examples of pictures taken under various conditions.

Figure 14 is a plot of the number of bubbles versus the size for various conditions. Figure 19 is a plot of some of the better experimental data along with the predicted void volumes which are calculated by a method explained in a later section.

Runs were made at 500, 1000, and 1500 psi for velocities of 20 and 30 ft/sec for various subcoolings. For most of this data the channel height was 0.5 inches though several runs at 0.18 inches and 0.09 inches were made. For this test strip under these conditions the void volume appeared to be independent of the channel height. This observation is consistent with the use of Equation (1) for calculating the incipient boiling points for all channel heights.

F. DISCUSSION

It is apparent that there is considerable scatter in the data. The principal cause of this is felt to be the difficulty in measuring a dimension then cubing it to determine a volume. For these relatively small vapor volumes, however, it does not appear that any other technique will yield a more accurate answer. This photographic procedure had the additional virtue of yielding information about the structure of the flow.

TABLE 1

Summary of the Void Volume Data

P		q/A	T_c	V_1	Measured	Calculated
lb/in^2		$\frac{BTU}{hr\ ft^2} \times 10^{-6}$	°F	ft/sec	a	a
500		0.52	450	20	1.75	0.84
500		0.44	441	20	0.075	0.221
500		0.54	441	20	0.170	0.314
500		0.77	425	20	0.68	0.378
500		1.2	400	20	0.78	0.183
500		1.44	400	20	1.21	0.254
500		2.02	350	20	0.67	0.151
500		2.32	350	20	0.85	0.20
500		0.59	450	30	0.36	0.39
500		0.78	450	30	1.26	0.59
500		1.0	425	30	0.125	0.136
500		1.25	425	30	0.140	0.21
500		1.25	400	30	0.080	0.064
500		1.49	400	30	0.105	0.103
500		1.65	400	30	0.360	0.129
500		1.78	375	30	0.090	0.090
500		2.00	375	30	0.103	0.118
500		2.06	350	30	0.05	0.054
500		2.44	350	30	0.14	0.078
1000		0.32	535	30	0.81	0.98
1000		0.45	535	30	0.87	1.67
1000		0.63	535	30	2.22	2.58
1000		1.04	498	30	0.25	0.229
1000		1.30	498	30	0.54	0.375
1000		1.90	448	30	0.15	0.136
1000		2.22	448	30	0.15	0.201
1000		0.25	535	20	0.94	1.44
1000		0.30	535	20	1.06	1.88
1000		0.38	535	20	1.06	2.60
1000		0.61	525	20	0.99	1.20
1000		0.81	525	20	2.97	1.72
1000		1.03	525	20	2.84	1.65
1000	*	0.47	517	20	0.16	0.33
1000	*	0.53	517	20	0.36	0.44
1000	*	0.71	517	20	0.85	0.74
1000		0.80	500	20	0.34	0.32
1000		1.28	500	20	2.11	0.75
1000	*	0.76	494	20	0.16	0.193
1000	*	1.03	494	20	0.32	0.40
1000		1.04	475	20	0.34	0.415
1000		1.25	475	20	0.58	0.284
1000		1.54	475	20	0.78	0.434

TABLE 1 (continued)

P	q/A	T_c	V_1	Measured	Calculated
lb/in²	$\frac{BTU}{hr\ ft^2} \times 10^{-6}$	°F	ft/sec	a	a
1000	1.52	450	20	0.17	0.206
1000	1.82	450	20	0.92	0.309
1000	2.15	450	20	0.83	0.424
1500	1.01	550	20	0.265	0.575
1500	1.25	550	20	0.360	0.83
1500	1.67	502	20	0.302	0.316
1500	1.97	502	20	0.535	0.451
1500	2.31	502	20	1.04	0.597
1500	2.27	450	20	0.135	0.215
1500	2.70	450	20	0.36	0.335

* 0.18" channel height

TABLE 2

Pressure lb/in^2	Velocity ft/sec	h BTU/hr ft^2 °F x 10^{-3}
500	20	9.26
500	30	12.9
1000	20	10.0
1000	30	12.9
1500	20	10.3

Film coefficients calculated from Equation 1

II THE PREDICTION OF VOID VOLUMES IN SUBCOOLED BOILING SYSTEMS

To begin, let us divide the boiling region in the channel into two parts. In the first part the net rate of change of vapor generation per unit length is negligible. In the second part the rate of increase in the void volume is sufficiently large so that the rate of change of void volume per unit length must be included in the heat balance on the test section. In Figure 15 a drawing of void volume per unit area is presented showing these two regions. We shall begin by considering each of the two regions separately, then combine the analysis so that a plot of void volume versus length can be developed for any heat flux and channel for specified conditions of inlet velocity or temperature.

A. The First Region

Photographs such as are shown in Figures 10, 11, 12, and 13 indicate that in the first region the vapor on the surface is in the form of a number of small bubbles which side view photographs show do not penetrate far into the subcooled liquid flowing over the surface. Under these conditions then there is a stratified flow pattern. In this region, it is also apparent that the total heat flux is larger but of the same order of magnitude as the heat flux that would exist if no boiling were present for the same conditions of velocity, subcooling, and surface temperature. That is, these pictures have been taken near the knee of the boiling curve before "fully developed" boiling has been established. In an earlier work (11) it was found in this region that the boiling heat flux vs ΔT could be correlated as if there were no forced convective heat transfer present as long as the forced convective heat flux were subtracted out. Therefore, let us use this notion to define a boiling heat flux

$$(q/A) = (q/A)_{nb} + (q/A)_b \qquad (2)$$

The non-boiling heat flux is obtained from the appropriate film coefficient by means of this equation.

$$(q/A)_{nb} = h(T_s - T_c) \qquad (3)$$

The physical justification for separating these two heat fluxes in this manner is indicated in Figures 10, 11, 12, and 13 where it is apparent that part of the surface is bare. The bare portions of the surface are most likely transferring heat more or less as it would if no boiling at all were present anywhere on the strip.

The saturation temperature is used in Equation (3) rather than the true wall temperature as, in general, the true wall temperature is not known with any precision and is only slightly higher than the saturation temperature. Let us now continue by considering how this boiling heat flux can be related to the void volume.

Begin by placing the steady flow energy equation on a system consisting initially of liquid at T_c and vapor and finally of just vapor. This is illustrated in Figure 17. For a unit depth the result is

$$\frac{q}{A}_b - \frac{q}{A}_c = \frac{(h_g - h_c)}{v_g} \frac{d(Va)}{dz} \qquad (4)$$

If there is no net vapor generation at the surface the"a" and the"V" are both constant so that the product (aV) is constant. For these conditions then, the right hand side of Equation (4) is 0 so that

$$(q/A)_b = (q/A)_c \qquad (5)$$

This is approximately true when the liquid is highly subcooled so that $(q/A)_c$ and $(q/A)_b$ are much larger than the enthalpy flux on the right. It is this assumption more than any other that limits the range

of application of this analysis. The next step is to consider what determines the rate at which vapor is condensed.

Consider now a number of bubbles of average diameter D_b. As the bubbles condense the condensing heat flux per unit of surface area is

$$\left(\frac{q}{A}\right)_c = \frac{n}{A} (\pi D_b^2) \, k \left(\frac{dT}{dr}\right)_{\text{bubble surface}} \qquad (6)$$

where D_b and (dT/dr) are "average" values. However, the void volume per unit area is related to the size and the number of bubbles per unit of area by the relation

$$a = \frac{n}{A} \pi \frac{D_b^3}{6} \qquad (7)$$

A relation exists between the average bubble size and the temperature gradiant at the wall. An easy method of obtaining this expression is as follows. Consider a bubble of initial diameter D_b' surrounded by subcooled liquid at T_c. When the bubble is partially condensed so that its diameter is bD_b' the enthalpy lost by the condensed vapor will appear as an increase in the temperature of the surrounding liquid. Assume the heated liquid layer surrounding the bubble has the thickness "δ" and is at an average temperature $(T_s + T_c)/2$. For values of b close to 1, the first law yields

$$\frac{\pi}{6} (D_b'^3 - b^3 D_b'^3) \frac{h_{fg}}{v_g} = \pi b^2 D_b'^2 \delta \, \frac{(T_s - T_c)}{2} \frac{c_l}{v_f}$$

Solve this for $1/\delta$ and the result is

$$\frac{1}{\delta} = \left(\frac{1 - b^3}{3b^2}\right) \frac{1}{D_b'} \, \frac{v_g c_l (T_s - T_c)}{v_g h_{fg}}$$

The function of "b" in the above expression varies between 1 and 0 for all condensing bubbles. If it is assumed that the same average value of

the function can be used for all bubbles, the average temperature gradiant at the wall becomes

$$\frac{dT}{dr} = B_o \left(\frac{T_s - T_c}{D_b} \right) \frac{v_g c_l (T_s - T_c)}{v_f h_{fg}} \qquad (8)$$

Equation (8) is essentially a definition of a constant B_o, which in this form should be independent of pressure or fluid properties.

When Equations (7) and (8) are substituted back in Equation (6) and all the constant quantities collected, the result is

$$\left(\frac{q}{A}\right)_c = \left(\frac{6B_o}{\pi}\right)\left(\frac{a}{D_b}\right)\left[\frac{k(T_s - T_c)}{D_b}\right]\left[\frac{v_g c_l (T_s - T_c)}{v_f h_{fg}}\right] \qquad (9)$$

We shall continue by considering how to evaluate an appropriate bubble diameter.

In reference (7) it was found that at elevated pressure for a highly subcooled bulk temperature, the size a bubble attains on a surface is proportional to the thickness of the layer of superheated liquid on the surface. As the surface is not completely covered by bubbles, this superheated liquid thickness is closely related to the film coefficient for heat transfer. This would not be true at either low velocity, low pressures, or at heat fluxes high enough so that more than a few layers of bubbles were on the surface. Let us assume then that the thermal layer thickness on the surface is proportional to k/h and the fraction of this layer which is superheated is $(T_w - T_s)/(T_w - T_b)$. Then it can be said

$$D_b \propto \frac{k}{h} \left(\frac{T_w - T_s}{T_w - T_c} \right) \qquad (10)$$

When Equations (10) and (5) are substituted in Equation (9) and the constant of proportionality and various other constants collected, the

result is

$$a = \frac{(q/A)_b}{\left[B_1 \left(\frac{v_g c_l (T_s - T_c)}{v_f h_{fg}}\right) \frac{(T_s - T_c)(T_w - T_s)h^2}{(T_w - T_c)\,k}\right]} \qquad (11)$$

This is the desired expression. The B_1 has been evaluated by selecting the value which best fits the data tabulated in Table 1. A comparison of the measured and calculated values of "a" is shown in the last two columns. The value of B_1 found to fit the data best is

$$B_1 = 2.0 \qquad (12)$$

In this expression, the T_c is evaluated as the mixed mean temperature for the liquid.

B. Evaluation of the Wall Superheat

In order to obtain values of the void volume which are correct, it is necessary to use the same values of the wall superheat which were used to obtain the constant B_1. The problem of the appropriate wall superheat is a difficult one and has not been satisfactorily solved for all possible conditions of surface, heat flux, and pressure. In view of these difficulties, it was felt a reasonable, direct and simple approximation was superior to an involved calculation based on doubtful premises. Therefore, the following procedure for obtaining the wall superheat has been used.

In reference (9) a curve is presented showing $(T_w - T_s)$ vs P/P_c for various fluids at the burnout point. This wall superheat is the maximum that would be obtained in nucleate boiling so it was assumed that half of the value from this curve was a good characteristic value to use. It was assumed, in addition, that this value was constant, independent of anything but critical pressure ratio. Obviously, this cannot be correct,

nevertheless the correlation obtained was only slightly improved when a reasonable wall superheat dependence on heat flux was assumed. Therefore, the simple assumption was used. The assumed wall superheat temperatures are presented in Figure 16.

C. Relating Void Volume to the Length

Usually the test section is sufficiently long so that there is a substantial heating of the fluid along the length of it and it is desired to determine the void volume as a function of length. This can be done by means of a heat balance. Assume as the system a section of length "z" and half channel height "s". The vapor and liquid at each section have a velocity V which is the same for both the heat balance, yields the result

$$\frac{q/A}{G}\left(\frac{z}{s}\right) = c_l(T_c - T_l) + \frac{a}{s}\,\frac{V}{V_l}\left(\frac{v_f}{v_g}\right)\left[c_l(T_s - T_c) + h_{fg}\right] \qquad (13)$$

The first term is the net heat transfer per pound of material flowing. The second term is the change in the enthalpy it would experience in going from liquid at T_l to liquid at T_c, and the last term is the number of pounds of vapor formed per pound of liquid flowing times its enthalpy change in going from liquid at T_c to saturated vapor.

The velocity at the exit can be obtained from the continuity equation and the assumption that the velocities for both phases are identical. This is

$$\frac{V}{V_l} = \frac{1}{\left(1 - \frac{a}{s}\right) + \frac{v_f}{v_g}\left(\frac{a}{s}\right)} \qquad (14)$$

When (14) is substituted into (13) and α is used to replace a/s, the result is

$$\frac{q/A}{G}\left(\frac{z}{s}\right) = c_l(T_c - T_l) + \frac{\alpha}{1 - \alpha(1 - \frac{v_f}{v_g})} \frac{v_f}{v_g}\left[c_l(T_s - T_c) + h_{fg}\right] \qquad (15)$$

Thus Equations (11) and (15) can be used to obtain the void volume-length relationships in the first region.

D. The Second Region

In the second region the surface is covered by several layers of bubbles. It therefore seems inappropriate to assume that every bubble is surrounded by liquid at T_c as only the top layers would see liquid at this temperature. The lower layers of bubbles would probably be close to T_s. Under these circumstances a different assumption is needed to relate the void volume to the heat flux. The assumption that has been made is, the area of condensing vapor no longer changes with length so that a constant magnitude condensing film coefficient "h_c" can be assumed. We shall continue by deriving the proper expression for the center temperature as a function of length, then by showing how the expressions for void volume for the two regions can be joined.

Define the constant condensing "h", which equals h_c, as follows:

$$(q/A)_c = h_c(T_s - T_c) \qquad (16)$$

If the steady flow energy equation is placed on the core of liquid, which is at T_c, and the weight of liquid that has been evaporated is assumed small compared to that remaining, the result is

$$\left(\frac{q}{A}\right)_c dz = \frac{sV_l}{v_f} c_l\,(dT_c) \qquad (17)$$

Substituting (16) into (17) and integrating from the transition distance z_t to distance "z", yields the result

$$h_c(z - z_t) = \frac{sV_l}{v_f} c_l \ln\left(\frac{T_s - T_{ct}}{T_s - T_c}\right) \qquad (18)$$

This relates the liquid temperature to the length beyond the transition point. Now we shall join the solutions.

An examination of the data of reference (6) indicates that when the boiling heat flux is approximately five times the forced convective heat flux the ln(q/A) vs ln(ΔT) curve no longer changes slope. This region can then be considered the region of "fully developed boiling." Therefore, it has been assumed that this is also the region in which the surface is virtually all covered with bubbles as the effects of the forced convection are no longer evident. That is when

$$(q/A)_b = 4(q/A)_{nb} \qquad (19)$$

The surface is at the transition point. In terms of film coefficients this becomes

$$h_c = 5h \qquad (20)$$

The liquid temperature at the transition point can be found by substituting (19), (20), and (3) in Equation (2). This temperature is T_{ct}. When this is done, the result is

$$T_{ct} = T_s - (q/A)(1/5h) \qquad (21)$$

The corresponding "a" can be found from Equation (11), and the corresponding length "z_t" from Equation (15). Thus, the appropriate values of length and liquid temperature can be found at any point. Actually, what is desired is the void volume at each point. This can be obtained by substituting the corresponding length and liquid temperature in Equation (15) and solving for α. It is therefore possible to calculate the void volume at every point. Let us now re-capitulate how a plot of

void volume vs length should be obtained for a given set of initial conditions and channel geometry.

E. Obtaining a Plot of Void Volume vs Length

Given information

1. Heat flux
2. Channel dimensions
3. Inlet velocity and temperature and the system pressure.

Steps

1. Calculate the film coefficient "h" that would exist with normal forced convective heat transfer in the absence of boiling.
2. Determine the temperature at which boiling starts from Equation (22). This is the point where "a" is 0.
3. Calculate transition liquid temperature "T_{ct}" from Equation (21).
4. Calculate the corresponding α from Equations (2), (3), (11), (12) and the definition of α.
5. Calculate z_t from Equation (15) in which $T_{ct} = T_c$.
6. Spot several values of α between the z where $\alpha = 0$ and where $z = z_t$ using Equations (3), (2), (11) and (12), and (15).
7. Start the calculation of a void volume in the second region by assuming a T_c which is greater than T_{ct} and substituting in Equation (18). This gives the appropriate value of z. z_t and T_{ct} have already been determined from steps 3, 4, and 5 above.
8. Calculate the corresponding α from Equation (15).

9. Calculate as many points as desired by going back to step 7 with a new value of T_c.

10. Plot α vs z, for the values determined from above and draw in a smooth curve.

Summary of Equations

$$q/A = h(T_s - T_c) \tag{22}$$

$$\alpha = a/s \qquad \text{(definition of } \alpha\text{)}$$

$$T_{ct} = T_s - (q/A)(1/5h) \tag{21}$$

$$q/A = (q/A)_{nb} + (q/A)_b \tag{2}$$

$$(q/A)_{nb} = h(T_s - T_c) \tag{3}$$

$$a = \frac{(q/A)_b}{2\left[\frac{v_g c_l (T_s - T_c)}{v_f h_{fg}}\right]\left[\frac{h^2 (T_s - T_c)(T_w - T_s)}{(T_w - T_c)\,k}\right]} \tag{11\&12}$$

$$\left(\frac{q/A}{G}\right)\frac{z}{s} = c_l(T_c - T_l) + \frac{\alpha}{1 - \alpha\left(1 - \frac{v_f}{v_g}\right)} \frac{v_f}{v_g}\left[c_l(T_s - T_c) + h_{fg}\right] \tag{15}$$

$$\frac{1}{G}\frac{z}{s} = \frac{c_{la}}{h_c} \ln \frac{(T_s - T_{ct})}{(T_s - T_c)} + \frac{z_t}{Gs} \tag{18}$$

F. Comparison with the Data

In reference (10) there are a number of curves presented for void volume data collected on a 2000 psia flowing system. The procedure outlined in the previous paragraphs has been used to calculate the void volumes under the stated conditions. The data has been plotted vs a fictitious quality rather than length, but the two are related through the following equation which is obtained from

$$x = \frac{\left(\frac{q/A}{G}\right)\left(\frac{z}{s}\right) + h_l - h_f}{h_{fg}} \tag{23}$$

the first law. The comparison of α's and x's, calculated using this procedure outlined here, with the experimental data, is shown in Figure 18.

It can be seen that, in general, the predictions are higher than the measurements. Part of this difference is due to the measurement technique used. Because there must exist a stratified flow pattern for the lower α regions, the gamma rays are likely to miss some of the vapor near the walls as the authors in reference (10) point out. This error approaches 28% in a stratified flow with small void volume. A 28% increase in the void volumes measured would bring the theory and experiments into good agreement for most of the runs shown.

It can be seen, though, on Figure 18 the runs with low velocities and heat fluxes the calculated α's are considerably higher than those observed. The reason for this discrepancy lies in the fact that in the first region it is assumed that all the heat transferred to the bubbles is condensed and therefore the enthalpy flux in the vapor is negligible. This assumption, embodied in Equation (5), is not true for low mass velocities and fluxes. Were the analysis to be extended to include all flux and flow conditions a lengthy trial and error procedure would be necessary in order to develop a α vs z curve so it has not been attempted. In any case, after solving the problem on the assumption that the boiling and condensing heat fluxes are equal, the resulting α vs z curve can be differentiated to obtain the size of the term set equal to 0 on the right of Equation (4) to determine the size of the error. It is because of this error that all the lower heat flux and mass velocity runs presented in reference (10) are omitted.

With the exception of liquid specific heat properties, all properties given in the equations in this work should be evaluated at the saturation temperature for the existing pressure unless the subscript indicates

otherwise. For the specific heat, in every case, it can be seen that it is immediately followed by a temperature difference. The specific heat should be evaluated as the mean value over that temperature difference.

G. Discussion

There are some limitations in this analysis. At low pressure the equation describing the bubble diameter, (10), becomes incorrect. This would become increasingly true below 0.1 of the critical pressure. The bubble diameter then becomes a function of pressure as well as the thickness of the superheated layer near the surface. The assumption that the right hand side of Equation (4) is 0 must be examined for each application. From these calculations it can be said that at lower vapor densities, higher velocities and higher heat fluxes, this assumption improves.

At this time it is difficult to evaluate the validity of the assumption that there is little slip between the phases. However, the data of reference (10) certainly implies this, though it is possible that the slip is greater than the 7 or 8% reported there. This is because, if the departures from equilibrium are sufficiently large, there is colder liquid and more vapor than the equilibrium assumption indicates. Under these circumstances, if the vapor could have a velocity substantially greater than that of the liquid yet the void volume would appear to be that existing for equilibrium conditions.

ACKNOWLEDGMENTS

The visual test section as well as much of the other test equipment in the visual system was designed by Mr. M. W. Raymond of the DIC Staff. The operation of the test stand and the photographic work was performed by George Henry. The bubble counting and the processing of the data was performed by Marlen L. Miller.

BIBLIOGRAPHY

1. Henry, George, "Density Variation in Water Flowing over a Flat Plate in Surface Boiling," S.M. Thesis, Department of Mechanical Engineering, M.I.T., May 1953.

2. Miller, Marlen L., "Pressure Drop in Forced Circulation Flow of Subcooled Water with and without Surface Boiling," S.M. Thesis, Department of Mechanical Engineering, M.I.T., August 1953.

3. Whitehead, Andrew L., "An Examination of Bubble Sizes Found in Local Boiling Heat Transfer Experiments," S.M. Thesis, Department of Chemical Engineering, M.I.T. July 1955.

4. Miller, Allen I., "Investigation of the Effect of Channel Height on the Density of Water Flowing Over a Flat Plate with Surface Boiling," S.M. Thesis, Department of Mechanical Engineering, M.I.T., May 1954.

5. Eckert, E. R. G., Introduction to the Transfer of Heat and Mass, McGraw-Hill Book Company, 1950.

6. Rohsenow, W. M., "A Method of Correlating Heat Transfer Data for Surface Boiling of Liquids," Trans. ASME, August 1952.

7. Griffith, Peter, "Bubble Growth Rates in Boiling," ASME Paper No. 57-HT-2, Presented August, 1957, at State College, Pennsylvania.

8. Forester, H. K., and N. Zuber, "Growth of a Vapor Bubble in a Superheated Liquid," Journal of Applied Physics, Vol. 25, 1954, pp 474-478.

9. Cichelli, M. T., and C. F. Bonilla, "Heat Transfer to Liquids Boiling Under Pressure," Trans. AIChE, Vol. 41, 1945, pp 755-787.

10. Egan, Richard A., David A. Dingee, Joel W. Chastain, "Vapor Formation and Behavior in Boiling Heat Transfer," Battelle Memorial Institute, ASME Paper 57-A-74.

11. Rohsenow, W. M., "Heat Transfer, A Symposium," 1952, Engineering Research Institute, U. of Michigan.

LIST OF SYMBOLS

A	Area
B_o	Dimensionless constant
B_1	Dimensionless constant equal to 2.0
D_b	Bubble diameter
G	Mass velocity
N_{nux}	Length Nussalt number, hz/k
N_{Rex}	Length Reynolds number, Gz/μ
N_{Pr}	Prandtl number, $c_l \mu/k$
P	Pressure
P_c	Critical Pressure
T	Temperature
T_l	Initial temperature
T_c	Mixed mean liquid temperature
T_{ct}	Mixed mean liquid temperature at transition
T_s	Saturation temperature
T_w	Wall temperature
V	Velocity
V_l	Initial velocity
a	Void volume per unit area
c_l	Liquid specific heat
c_{la}	Liquid specific heat evaluated as mean between T_c and T_{ct}
h	Film coefficient in the absence of boiling
h_c	Condensing film coefficient
h_f	Saturated liquid enthalpy
h_{fg}	Change in enthalpy from liquid to vapor
h_g	Saturated vapor enthalpy

LIST OF SYMBOLS (continued)

h_l	Initial liquid enthalpy
k	Liquid thermal conductivity
n	Number of bubbles
r	Radius of bubble
s	Channel spacing for one heated wall, 1/2 channel spacing for two heated walls
v_f	Liquid specific volume
v_g	Vapor specific volume
x	Equality
z	Length
z_t	Length at transition
q/A	Heat flux
$(q/A)_b$	Boiling heat flux
$(q/A)_c$	Condensing heat flux
$(q/A)_{nb}$	Non-boiling heat flux = $h(T_s - T_c)$
α	= a/s = void fraction

CAPTIONS

Figure 1 Diagram of visual test loop

Figure 2 Visual test section

Figure 3 Top view of visual test section. Top view pictures taken with camera at A, light source at B.

Figure 4 Visual test section window assembly

Figure 5 Visual test section window frame

Figure 6 Stainless steel reflector window

Figure 7 Dimensions of heater strip in inches

Figure 8 Diagram of heater strip

Figure 9 Visual test section back plate assembly

Figure 10 Boiling on the heater surface

$P = 500$ psi
$V = 30$ ft/sec
$T = 400$ °F
$(q/A) = 1.65 \times 10^6$ BTU/hr ft^2
$(a/A)_{nb} = 0.86 \times 10^6$ BTU/hr ft^2

Figure 11 Boiling on the heater surface

$P = 1000$ psia
$V = 30$ ft/sec
$T = 475$ °F
$(q/A) = 1.540 \times 10^6$ BTU/hr ft^2
$(q/A)_{nb} = 0.69 \times 10^6$ BTU/hr ft^2

Figure 12 Boiling on the heater surface

$P = 1000$ psia
$V = 30$ ft/sec
$T = 500$ °F
$(q/A) = 1.3 \times 10^6$ BTU/hr ft^2
$(q/A)_{nb} = 0.59 \times 10^6$ BTU/hr ft^2

CAPTIONS (continued)

Figure 13 Boiling on the heater surface

$P = 1500$ psia
$V = 20$ ft/sec
$T = 450$ °F
$(q/a) = 2.27 \times 10^6$ BTU/hr ft²
$(q/A)_{nb} = 1.5 \times 10^6$ BTU/hr ft²

Figure 14 Representative bubble spectrums

Case	P	V	$T_s - T_c$	q/A
	psia	ft/sec	°F	BTU/hr ft²
C	500	20	92	2.02×10^6
J	1000	20	70	1.25×10^6
N	1000	20	20	1.03×10^6
Q	1000	30	95	2.22×10^6
S	1000	30	97	1.82×10^6
Z	1500	20	144	2.70×10^6

Figure 15 Void volume vs length

First region - negligible enthalpy flux in the vapor
Second region - appreciable enthalpy flux in the vapor

Figure 16 Wall superheats for all fluids for substitution in Equations (11) and (12). (From reference 9.)

Figure 17 Control volume used in derivation of Equation (4). The surfaces with heat crossing have no flow crossing them.

Figure 18 Void volume vs fictitious quality from Reference (10). P = 2000 spi. Solid line is the equilibrium assumption with no slip, dashed line is the best line through the points, dash-dot line is the line from the analysis presented in this report.

Figure 19 Comparison of selected calculated and measured void volumes for data presented in Table 1. Solid lines are the plot of Equation (11) with $B_1 = 2.0$.

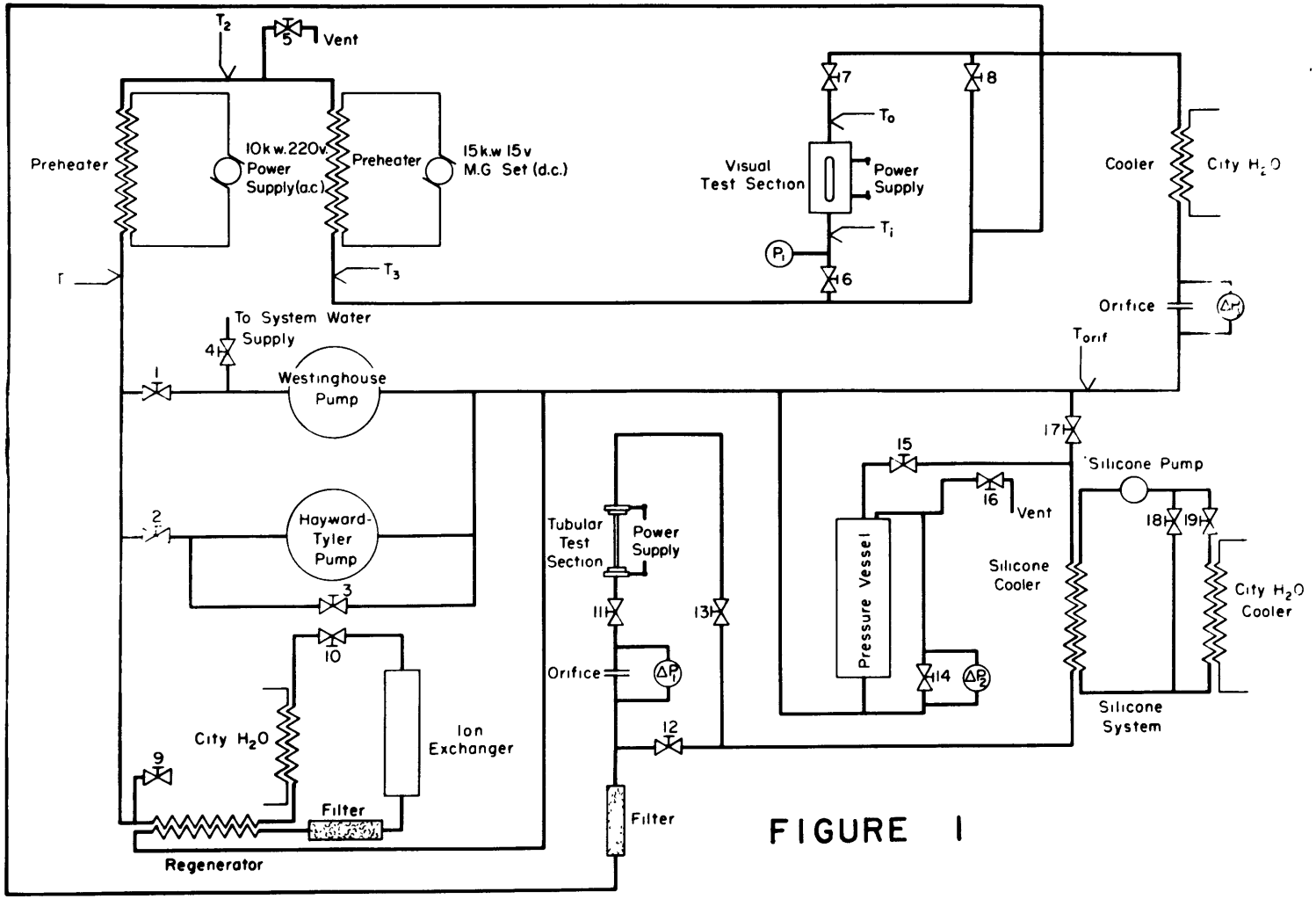
T2
5
Vent
Preheater
10k w. 220v. Power Supply (a.c.)
Preheater
15k.w 15v M.G Set (d.c.)
T3
7
8
To
Visual Test Section
Power Supply
Ti
Pi
6
Cooler
City H2O
Orifice
ΔP3
Torif
To System Water Supply
4
1
Westinghouse Pump
17
Silicone Pump
15
16
Vent
18
19
2
Hayward-Tyler Pump
3
Tubular Test Section
Power Supply
Pressure Vessel
Silicone Cooler
City H2O Cooler
11
13
10
Orifice
ΔP1
14
ΔP2
City H2O
Ion Exchanger
12
9
Filter
Filter
Silicone System
Regenerator

FIGURE 1

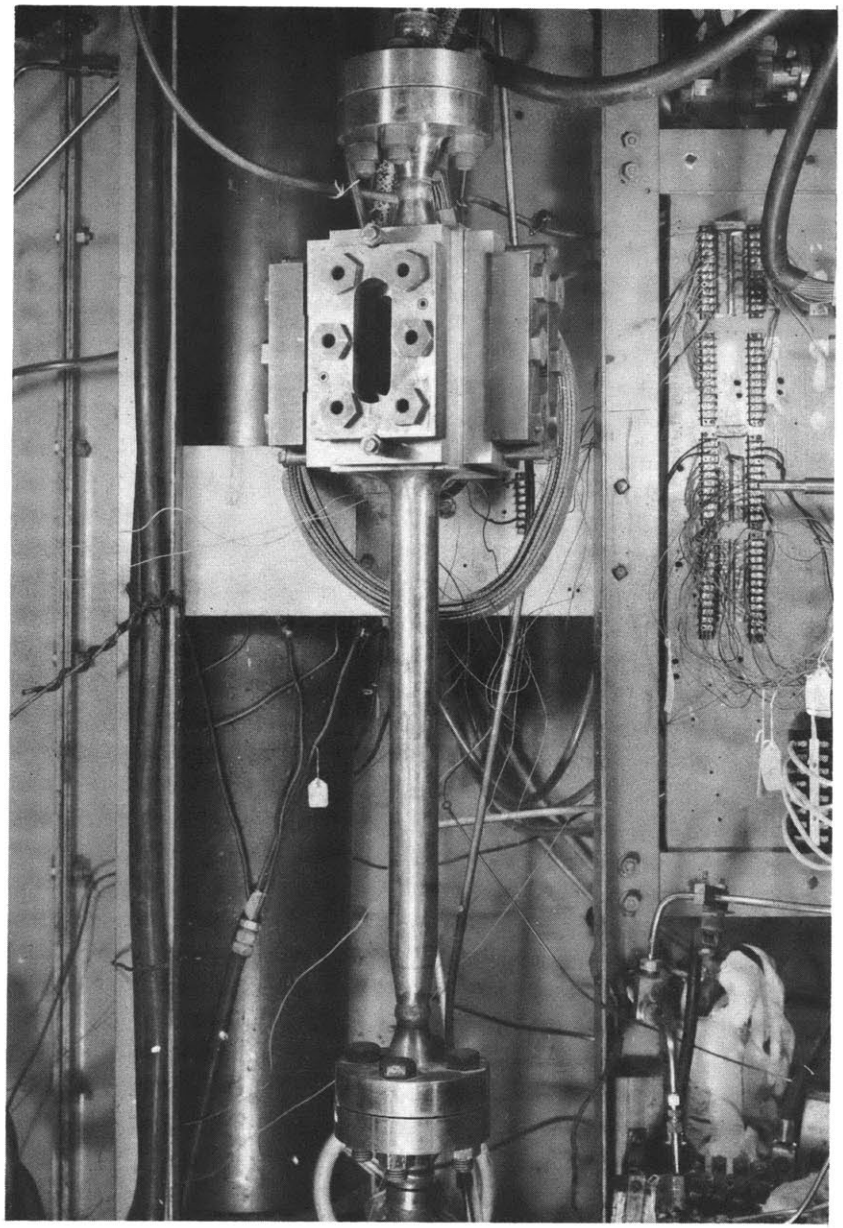

FIGURE 2

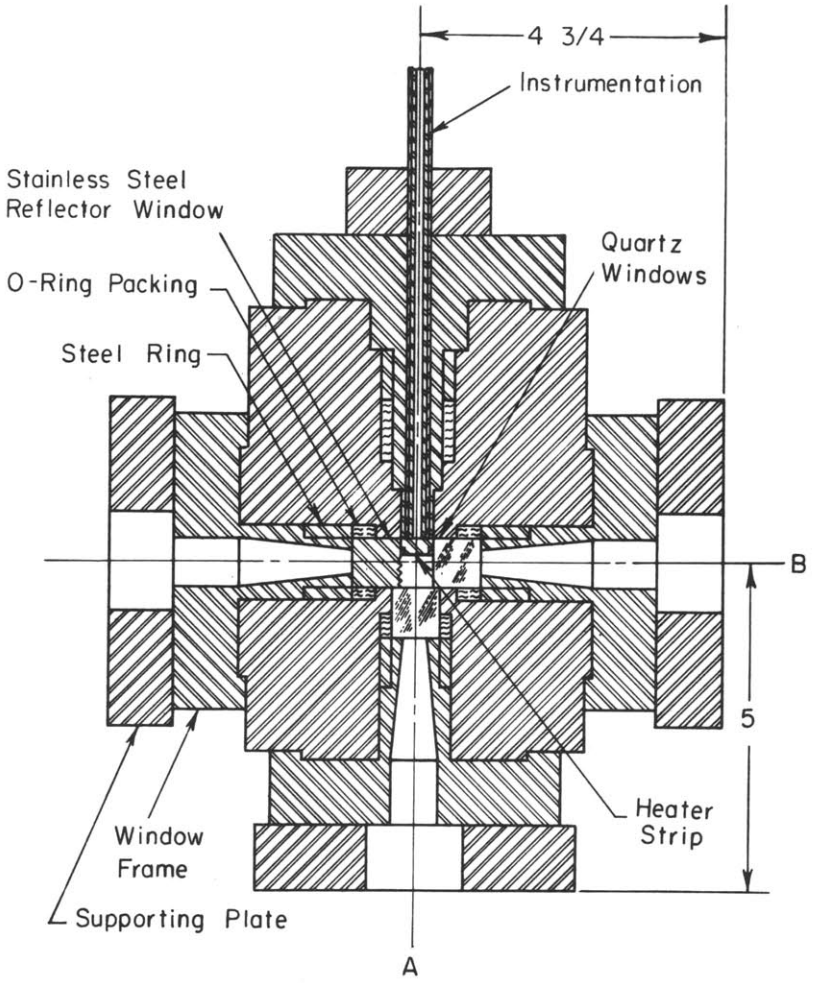

FIGURE 3

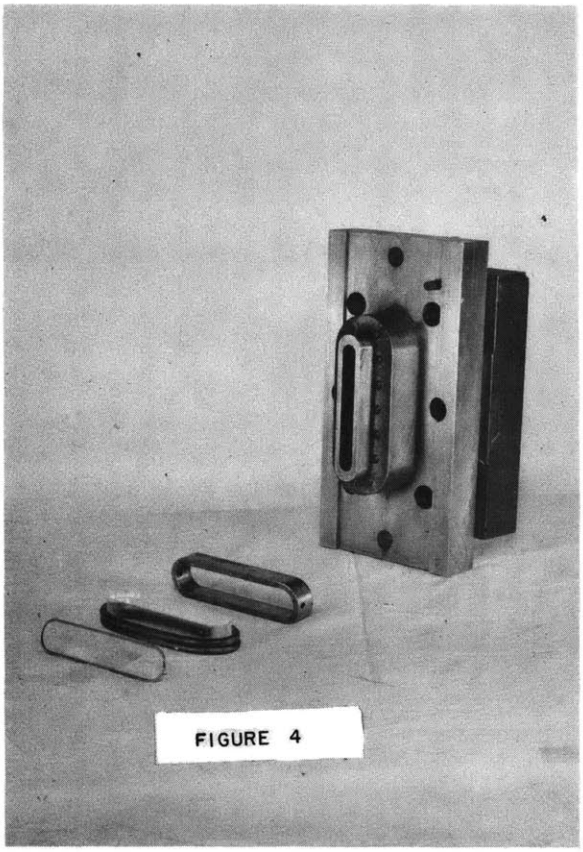

FIGURE 4

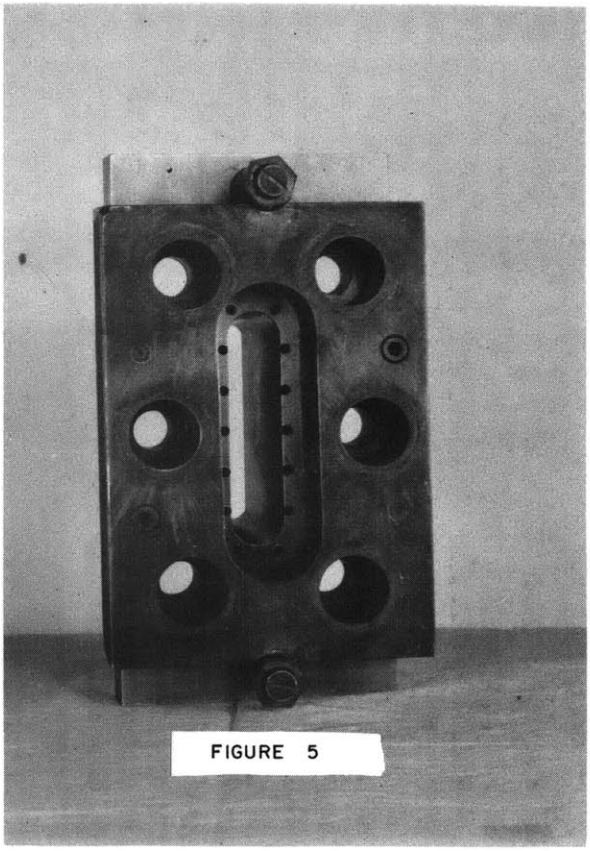

FIGURE 5

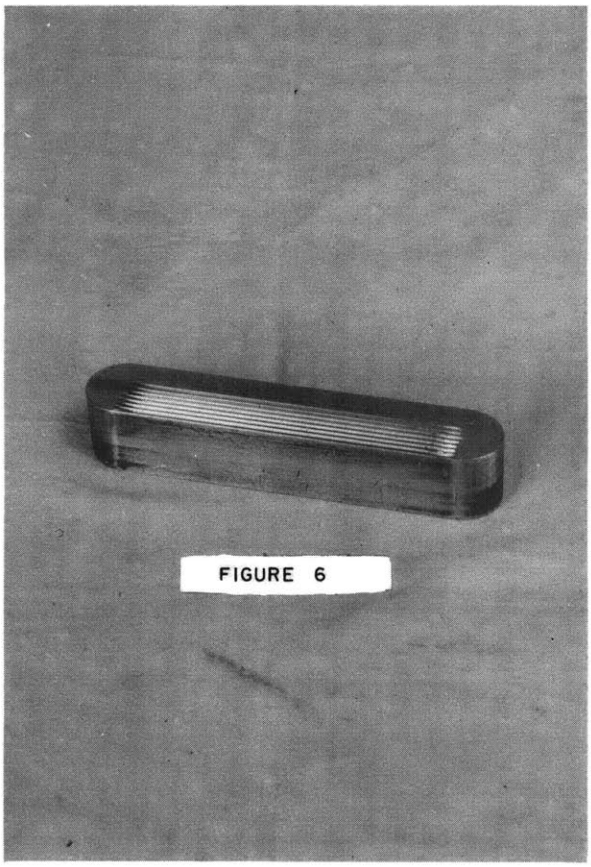

FIGURE 6

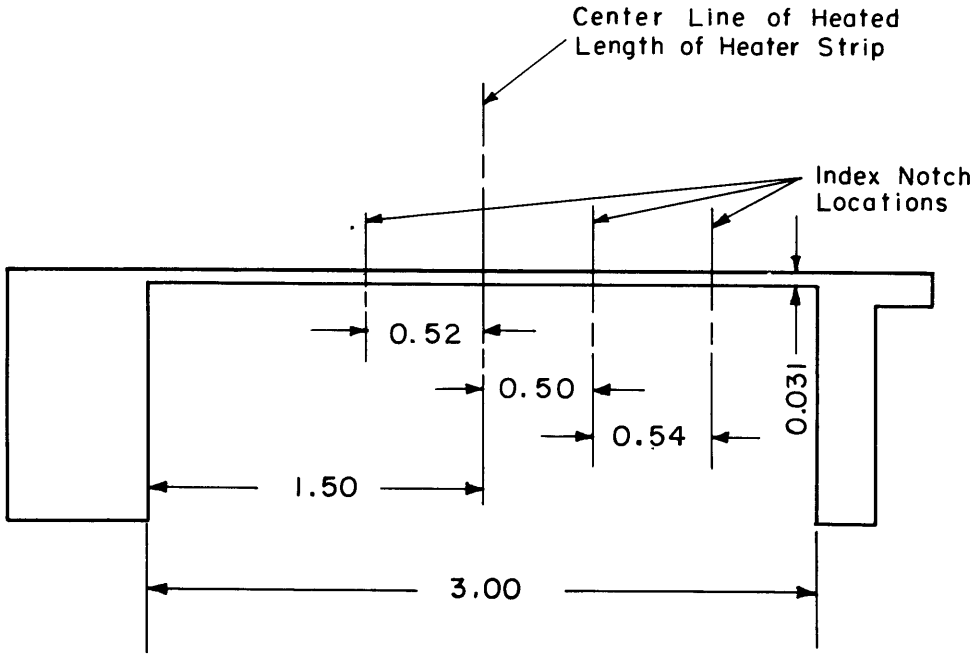

FIGURE 7. DIMENSIONS OF HEATER STRIP

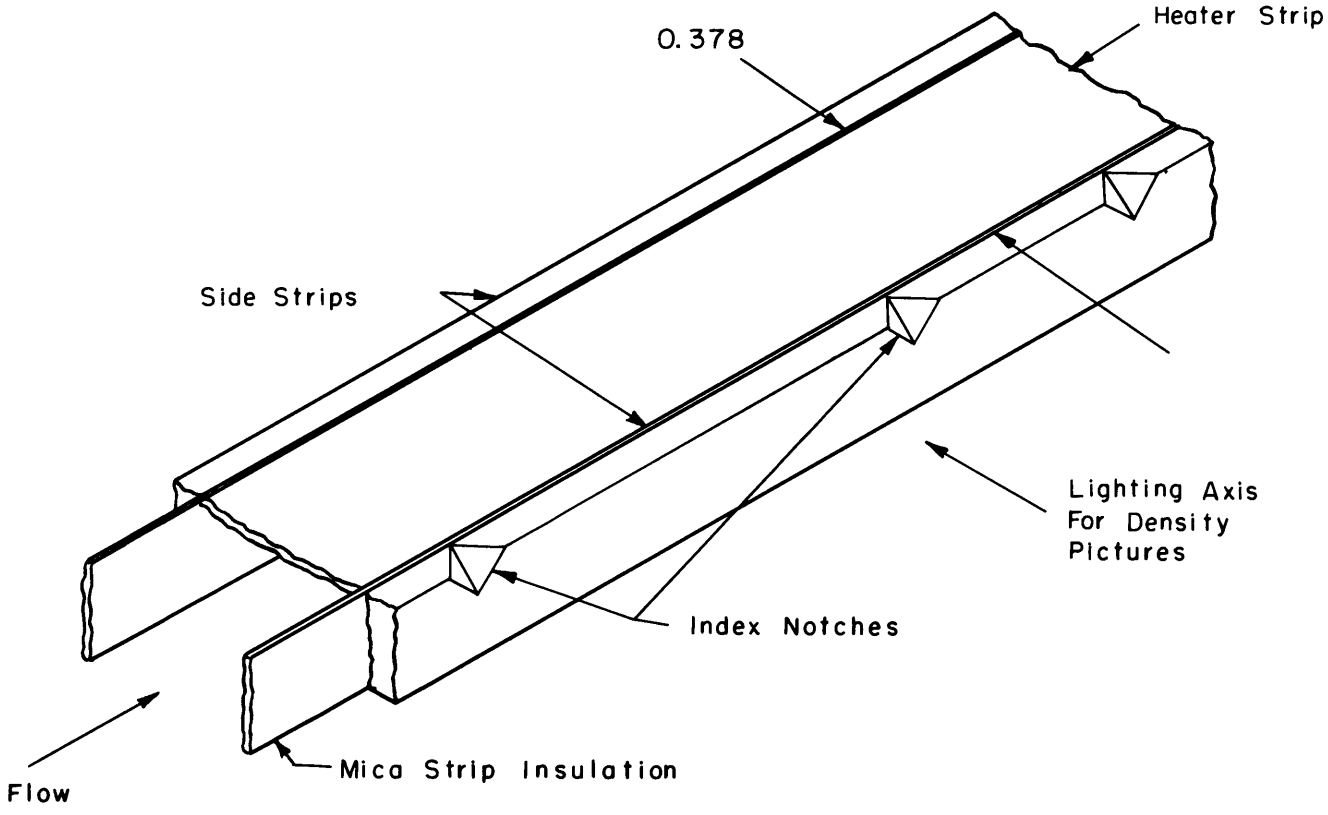

FIGURE 8 DIAGRAM OF HEATER STRIP

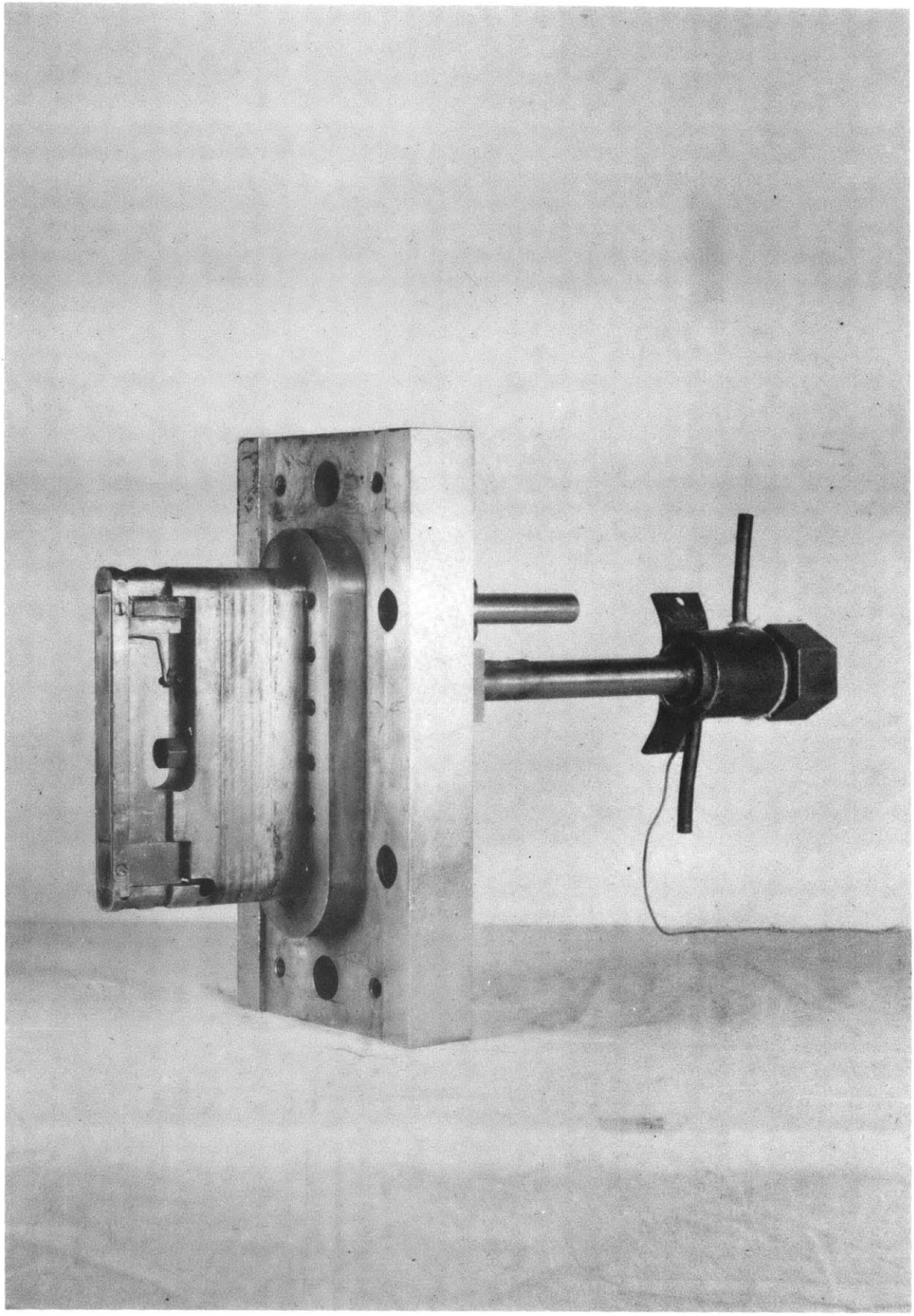

FIGURE 9

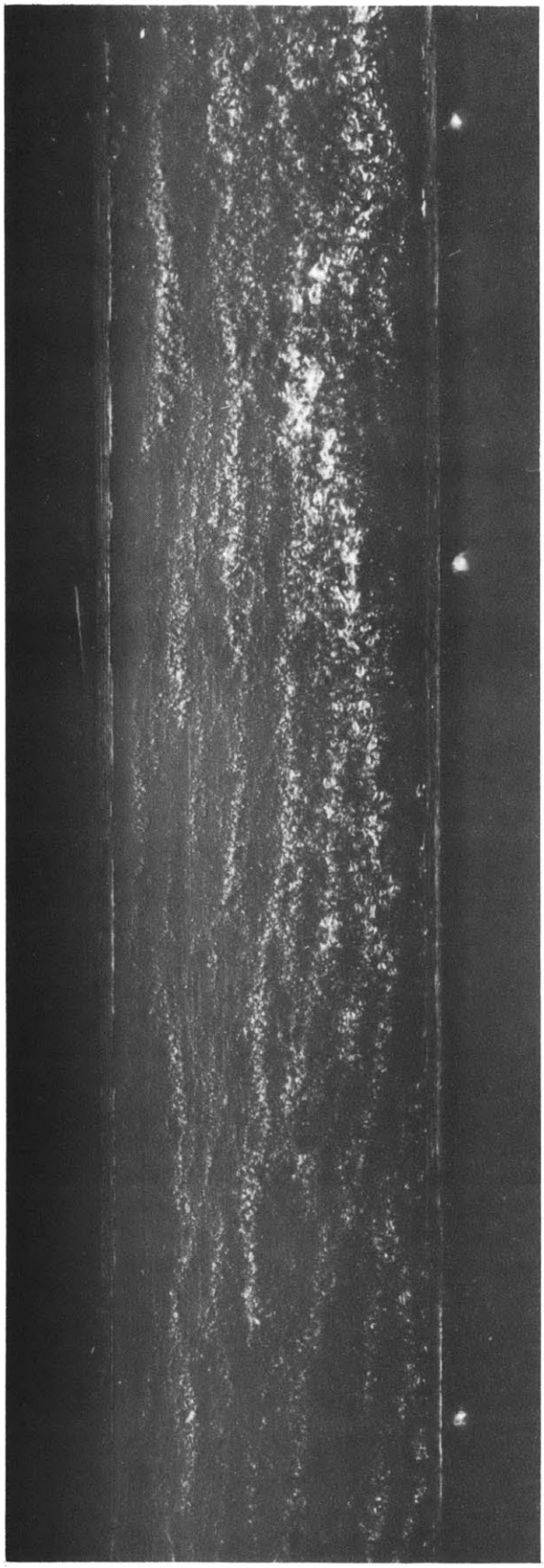

FIGURE 10

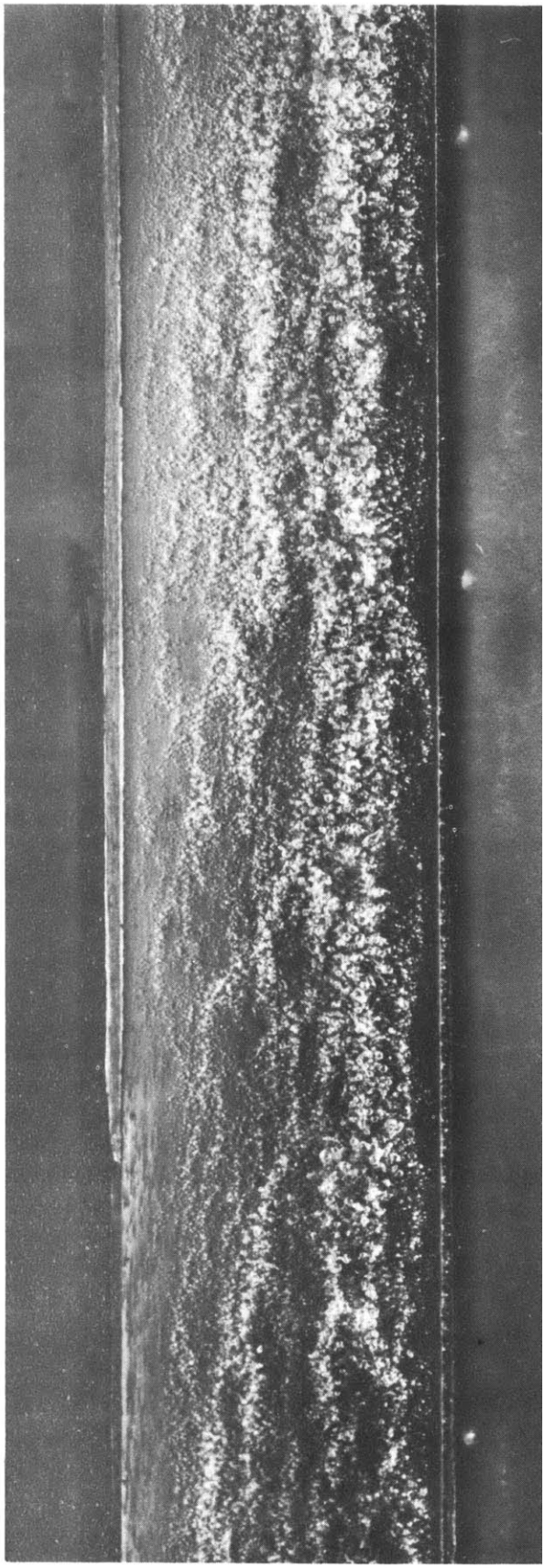

FIGURE 11

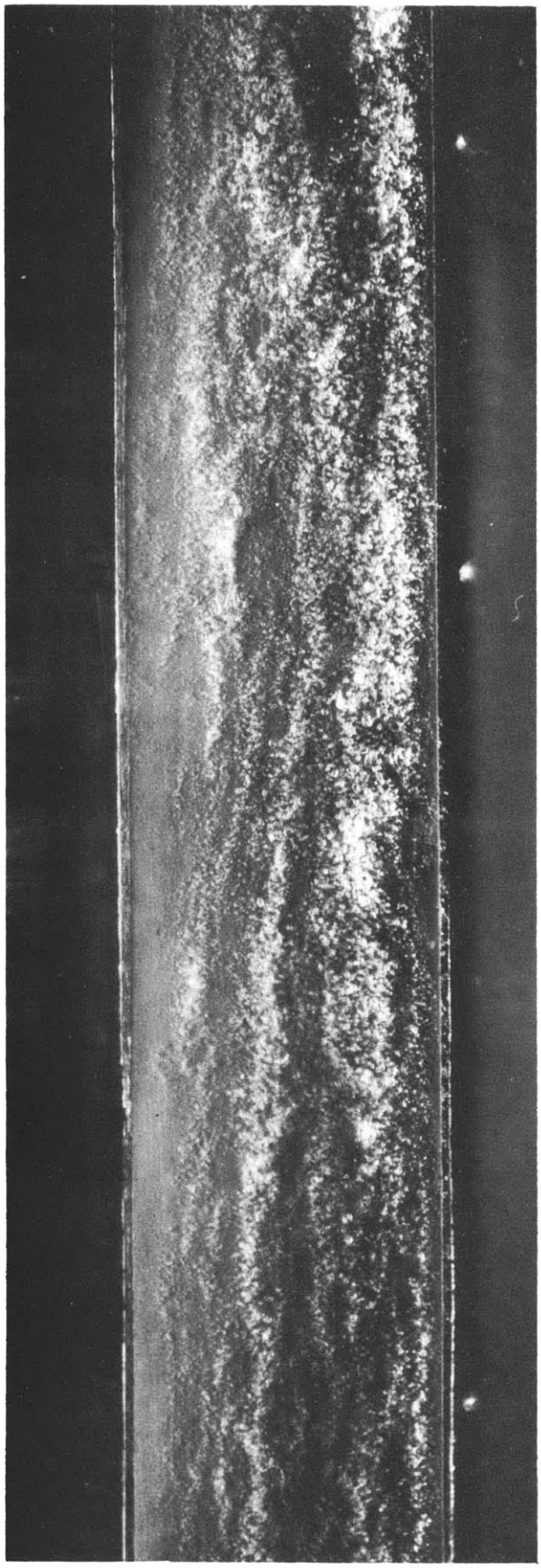

FIGURE 12

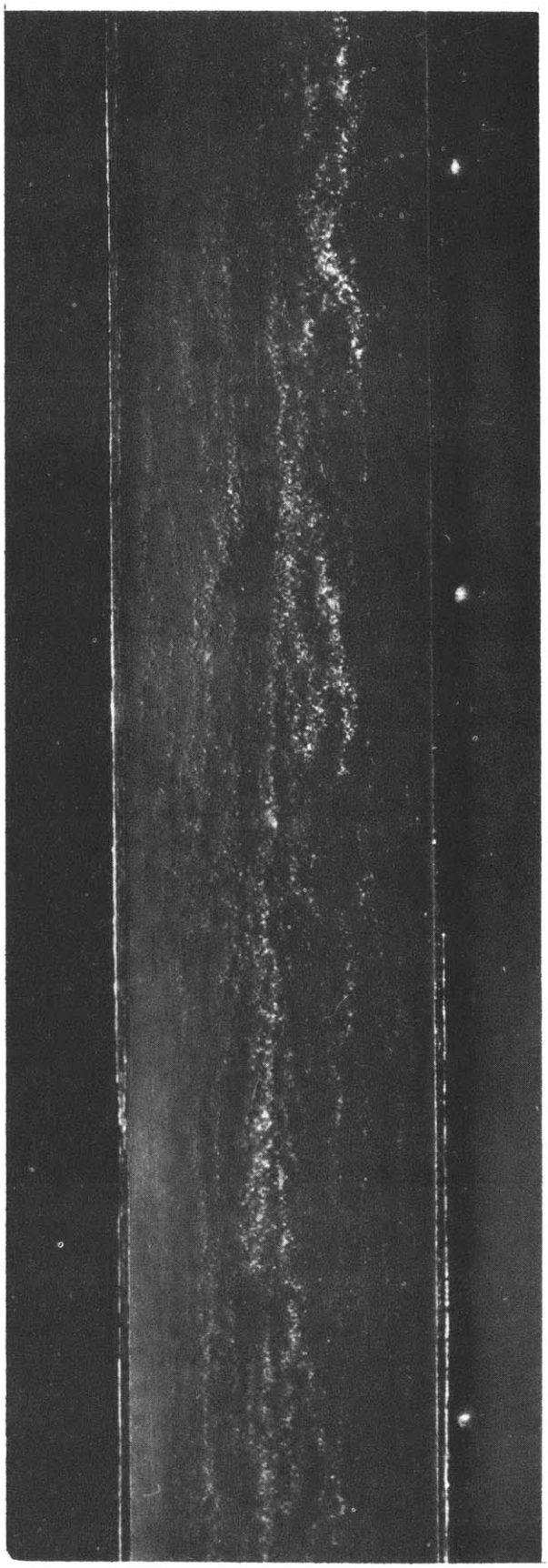

FIGURE 13

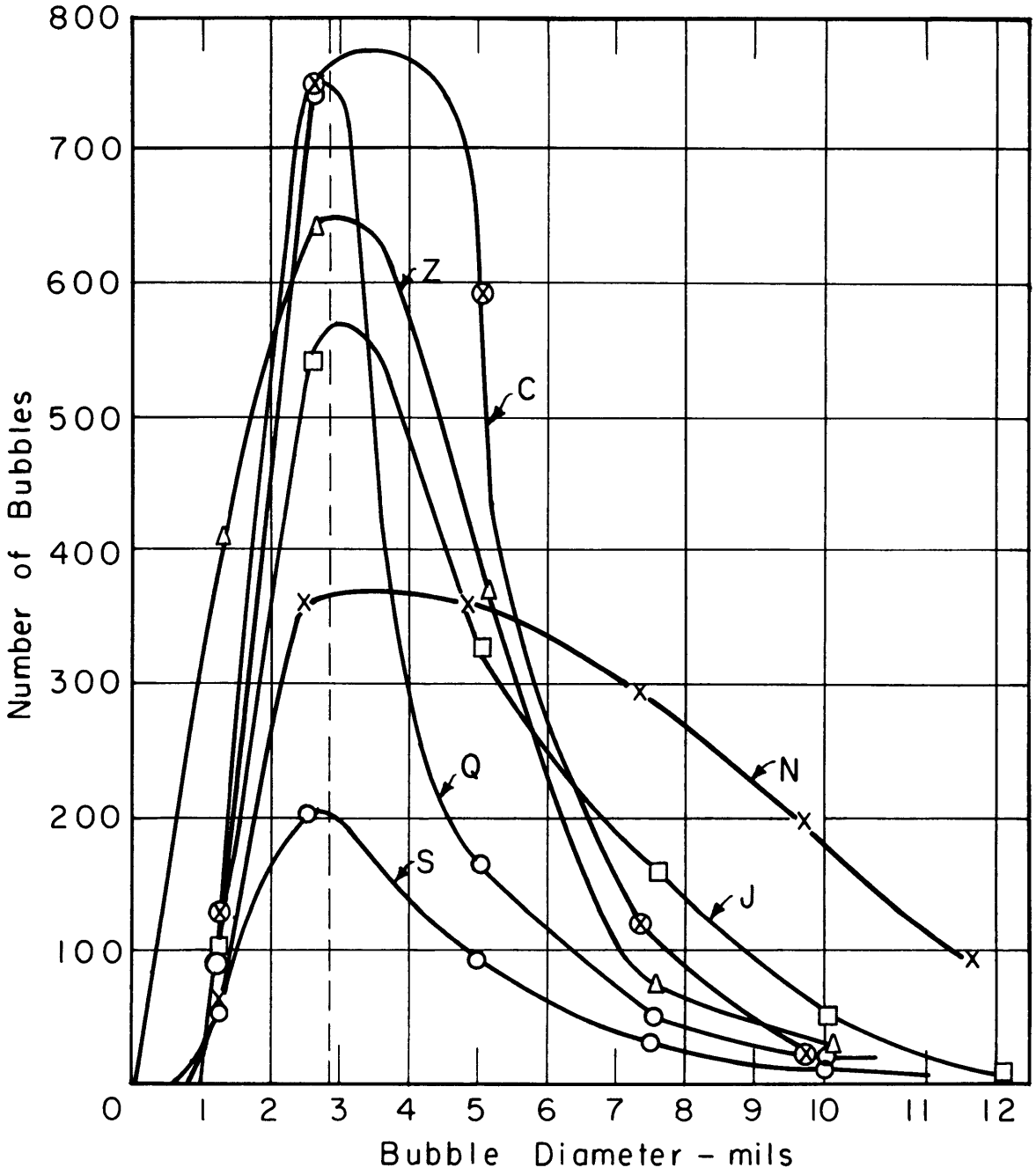
800
700
600
500
400
300
200
100
0
1
2
3
4
5
6
7
8
9
10
11
12
Number of Bubbles
Bubble Diameter – mils
Z
C
Q
S
N
J

FIGURE 14

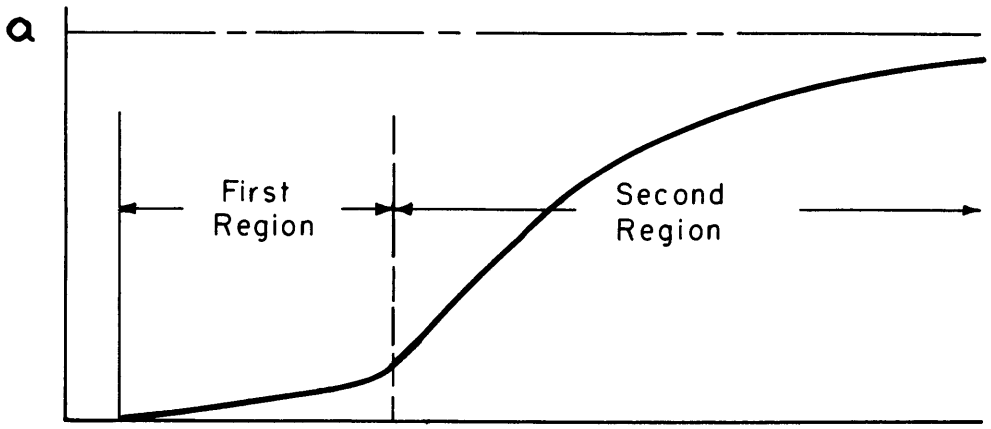

FIGURE 15

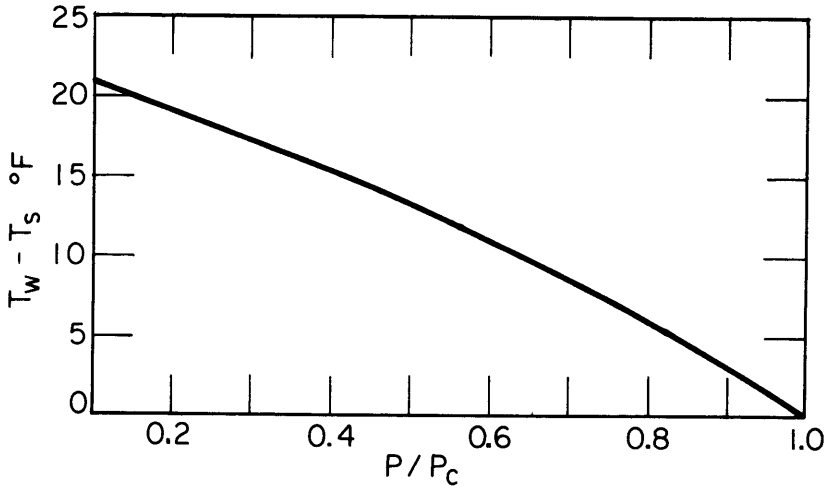

FIGURE 16

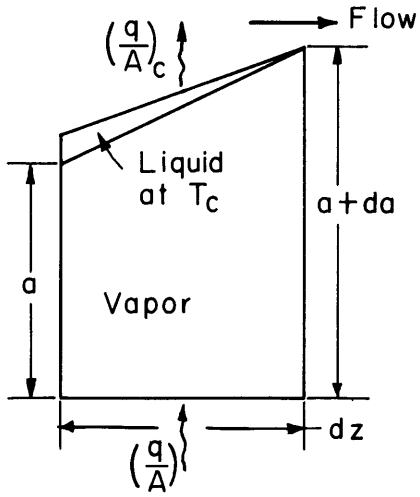

FIGURE 17

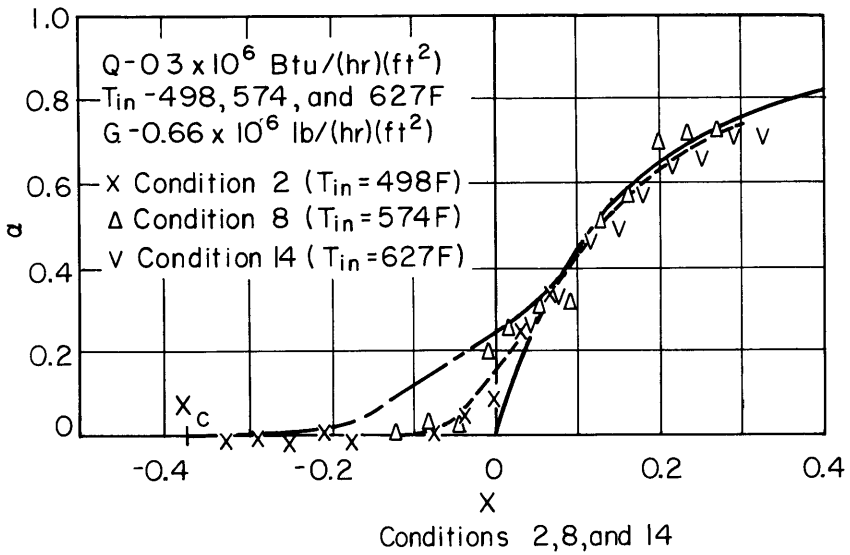

Conditions 2,8,and 14

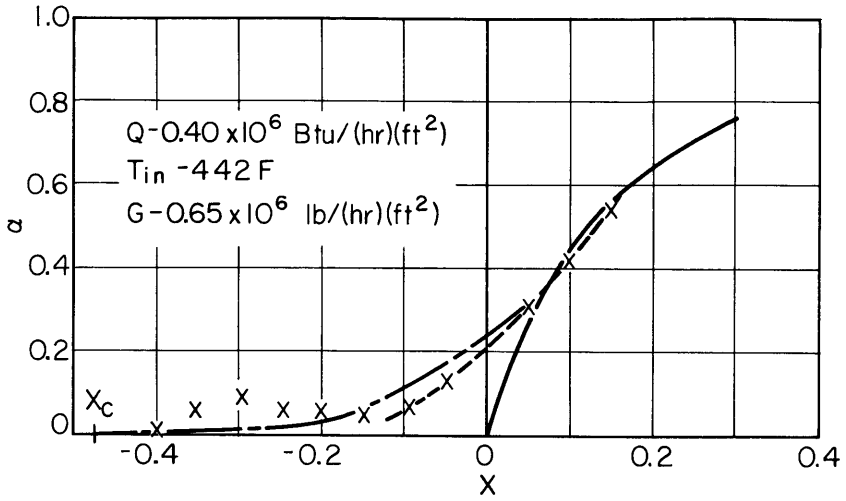

Condition B3 - 3

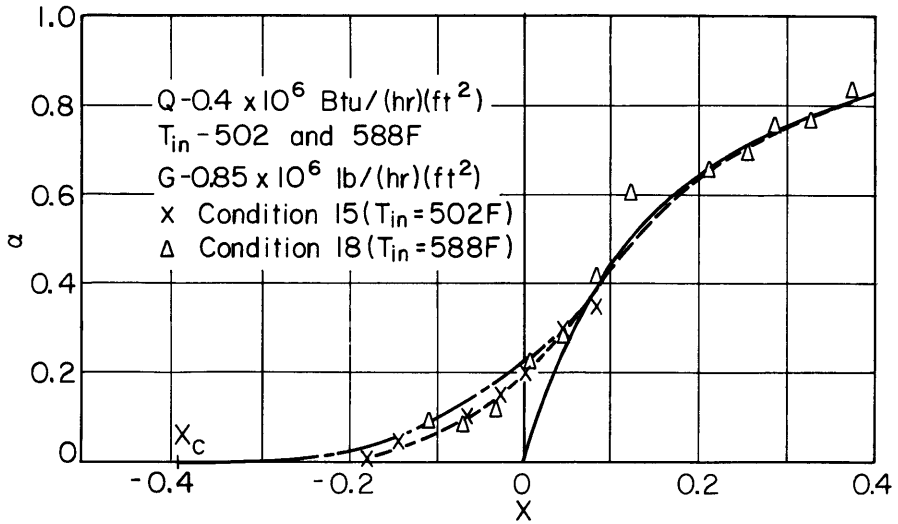

Conditions. 15 and 18

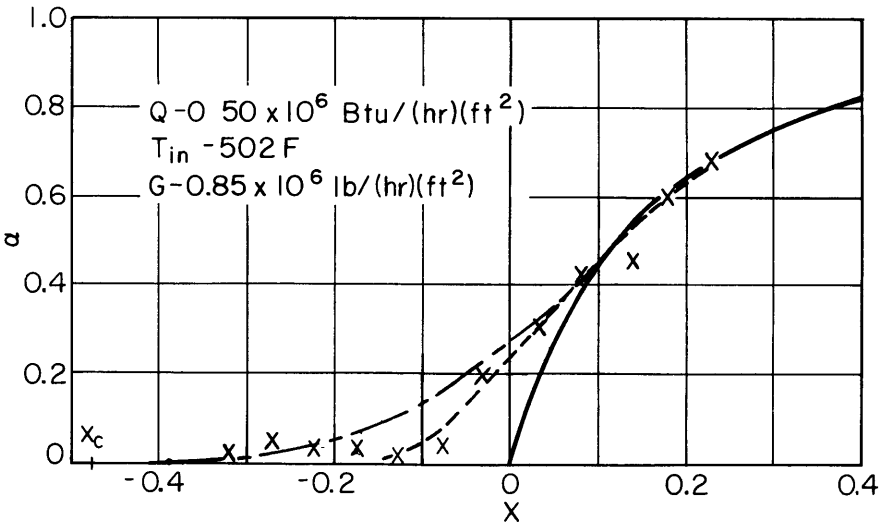

Conditions 16

FIGURE 18

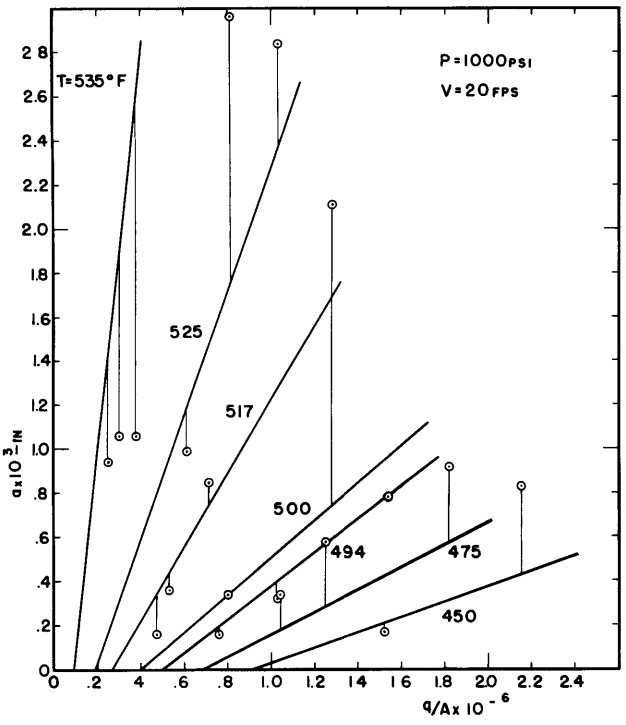
P=1000PSI
V=20FPS
T=535°F
525
517
500
494
475
450
a x 10^3 - IN
q/A x 10^-6

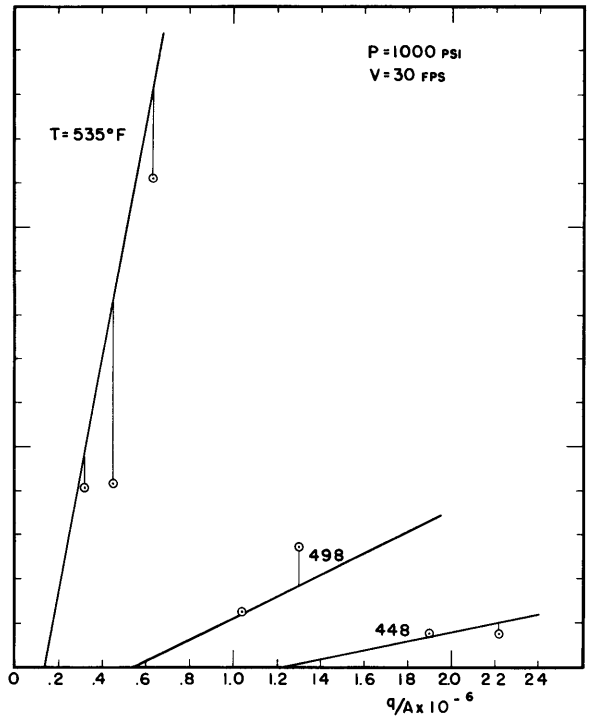
P=1000 PSI
V=30 FPS
T=535°F
498
448
q/A x 10^-6

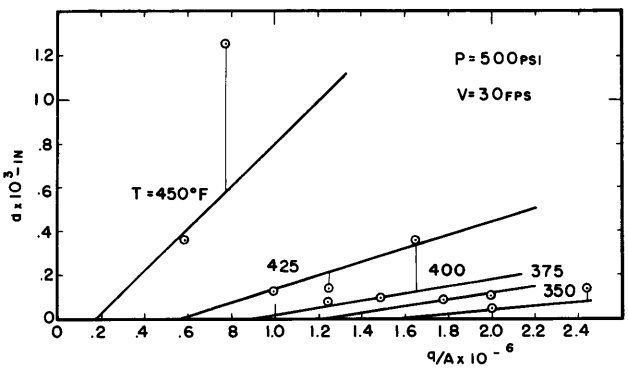
P=500PSI
V=30FPS
T=450°F
425
400
375
350
a x 10^3 - IN
q/A x 10^-6

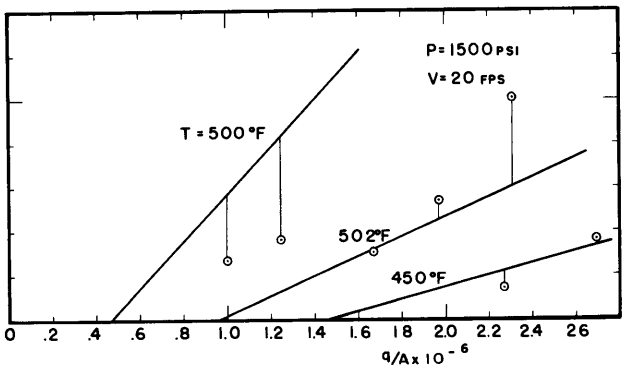
P=1500PSI
V=20 FPS
T=500°F
502°F
450°F
q/A x 10^-6

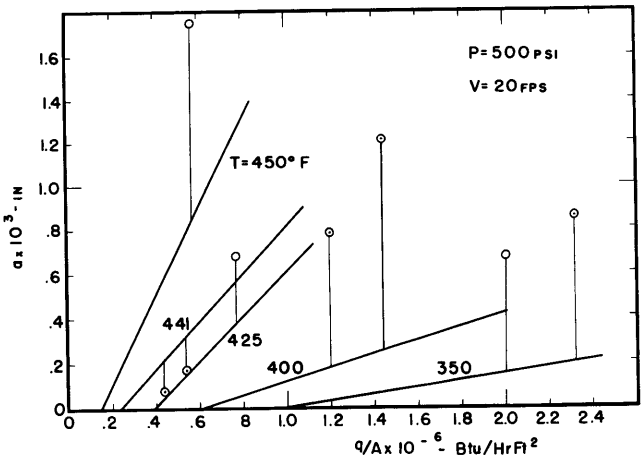
P=500PSI
V=20FPS
T=450°F
441
425
400
350
a x 10^3 - IN
q/A x 10^-6 - Btu/HrFt^2

FIG.19